AGU PUBLICATIONS

Radio Science

RESEARCH ARTICLE
10.1002/2016RS005953

Special Section:
Ionospheric Effects Symposium 2015

Generation of ELF waves during HF heating of the ionosphere at midlatitudes

A. S. Sharma[1], B. Eliasson[1,2], X. Shao[1], and K. Papadopoulos[1]

[1]Department of Astronomy, University of Maryland, College Park, Maryland, USA, [2]SUPA, Physics Department, University of Strathclyde, Glasgow, UK

Key Points:
- ELF generation in ionospheric heating in the midlatitudes
- Mode conversion of fast mode to shear Alfvén, EMIC, and whistler waves
- Relevant to ionospheric heating using Arecibo heating facility

Correspondence to:
A. S. Sharma,
ssh@astro.umd.edu

Citation:
Sharma, A. S., B. Eliasson, X. Shao, and K. Papadopoulos (2016), Generation of ELF waves during HF heating of the ionosphere at midlatitudes, *Radio Sci.*, *51*, doi:10.1002/2016RS005953.

Received 15 JAN 2016
Accepted 13 APR 2016
Accepted article online 22 APR 2016

Abstract Modulated high-frequency radio frequency heating of the ionospheric *F* region produces a local modulation of the electron temperature, and the resulting pressure gradient gives rise to a diamagnetic current. The oscillations of the diamagnetic current excite hydromagnetic waves in the ELF range that propagate away from the heated region. The generation of the waves in the 2–10 Hz range by a modulated heating in the midlatitude ionosphere is studied using numerical simulations of a collisional Hall-magnetohydrodynamic model. To model the plasma processes in the midlatitude ionosphere the Earth's dipole magnetic field and typical ionospheric plasma parameters are used. As the hydromagnetic waves propagate away from the heated region in the *F* region, the varying plasma conditions lead to changes in their characteristics. Magnetosonic waves generated in the heating region and propagating down to the *E* region, where the Hall conductivity is dominant, excite oscillating Hall currents that produce shear Alfvén waves propagating along the field lines into the magnetosphere, where they propagate as the electromagnetic ion cyclotron (EMIC) and whistler waves. The EMIC waves propagate to the ion cyclotron resonance layer in the magnetosphere, where they are absorbed.

1. Introduction

The heating of the ionosphere by high-frequency (HF) radio transmitters has been used to explore the ionosphere as a large-scale natural laboratory and to study many plasma processes. Along with the heating of the plasma many new phenomena have been discovered using the HF transmitters, including stimulated emissions [*Leyser*, 2001], excitation of plasma waves and turbulence [*Guzdar et al* 2000], modulation of the ionospheric current systems and associated controlled generation of low-frequency electromagnetic radiation [*Papadopoulos et al*., 1989; 2011a,2011b; *Stubbe*, 1996], small-scale irregularities or striations [*Gurevich et al*., 1996; *Mishin et al*., 2005], pump-induced optical processes [*Bernhardt*, *Tepley and Duncan*, 1989, *Pedersen and Gerken*, 2005], ion up flows in the topside ionosphere [*Kosch et al*., 2010; *Milikh et al*., 2010], and descending artificial ionospheric layers [*Pedersen et al*., 2010]. The generation and propagation of low-frequency hydromagnetic waves due to the HF heating are some of the key results of ionospheric heating experiments at High Frequency Active Auroral Research Program (HAARP) [*Papadopoulos et al*., 2011a, 2011b].

The low-frequency waves generated in the ionosphere during heating experiments with modulated HF waves (1–10 MHz) originate from three types of physical mechanisms. The first type of mechanism requires the presence of an electrojet current such as the auroral electrojet and relies on the modulation of the *D*/*E* region conductivity as a response to modulated HF heating. The resulting modification of the electrojet current creates an effective antenna radiating at the modulation frequency [*Stubbe et al*., 1981; *Papadopoulos et al*., 1989; Stubbe, 1996]. This mechanism of low-frequency wave generation by modulating the auroral electrojet is effective at ~80 km altitude in the *D*/*E* region and is referred to as the Polar Electrojet antenna. In the second type of mechanism the HF heating leads to a local hot spot and thus a region of strong gradient in the plasma pressure. This leads to a diamagnetic current that excites the hydromagnetic waves with the time scale of the modulation frequency. In this case there is no quasi-steady or background current, and the wave excitation is controlled by the parameters such as the plasma conductivity, HF modulation frequency, and size of the heated region. This mechanism has been studied in simulations for the *F* region of high-latitude ionosphere [*Papadopoulos et al*., 2011a, 2011b; *Eliasson et al*., 2012] for conditions typically corresponding to the HAARP facility. This mechanism, which has been verified by experiments at HAARP, has features such as scaling of the wave amplitude with frequency [*Papadopoulos et al*., 2011b]. The third type of mechanism of generating low-frequency waves is based on nonlinear interaction between the plasma and fields and was motivated in part by observations by the DEMETER satellite during experiments at HAARP with

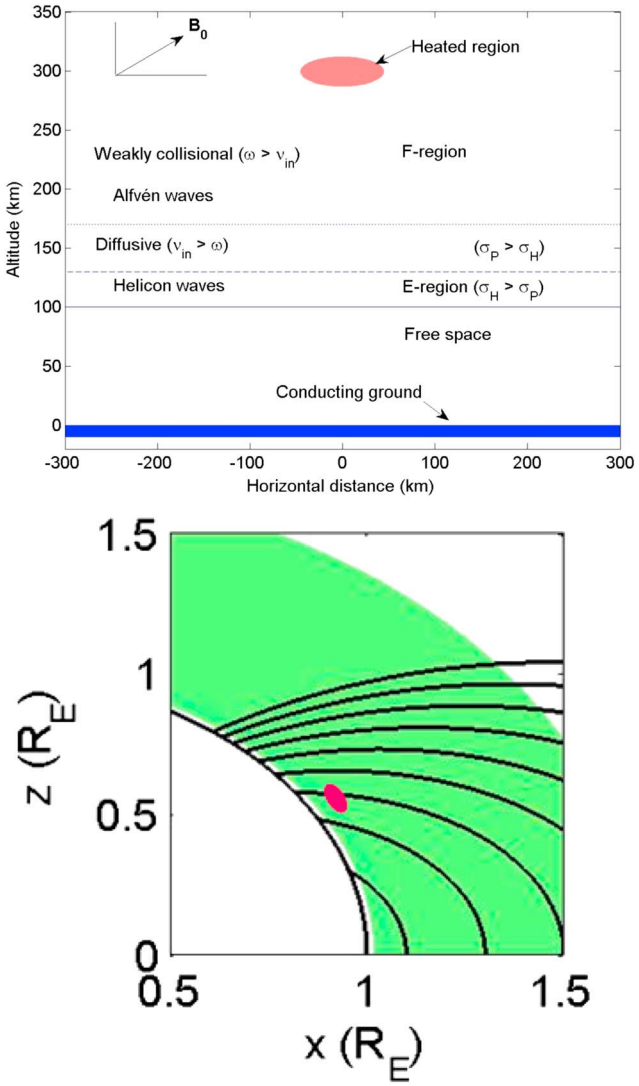

Figure 1. (top) Sketch of the ionosphere (above $z = 100$ km, with free space below and a conducting ground) and the regions characterized by the relative magnitudes of the Hall (σ_H) and Pederson (σ_P) conductivities. The space-dependent geomagnetic field $\mathbf{B}_0$ magnetizes the plasma. The heated region is located in the *F* region at an altitude of 300 km. (bottom) Part of the simulation domain (shaded in green) using polar coordinates in the midlatitude region with the Earth's dipole magnetic field the heated region (in red) is centered at the magnetic field line $L = 1.6$, with $R_E = 6000$ km.

no modulation of the HF power. These waves are generated by parametric processes and have been identified as whistlers with frequencies close to that of lower hybrid waves. In another mechanism that relies on nonlinearity, the interaction of two large-amplitude HF waves produce oscillations in electron temperature, and consequently in the collision frequency. The latter interact with the polarization current associated with the HF wave to produce ELF and VLF waves, which have been observed in HAARP experiments [*Moore et al.*, 2013].

In the high-latitude ionosphere Alfvén wave propagation is described by the MHD model, in which all plasma species are magnetized [*Lysak*, 1990]. However, in the *E* region altitudes of 80–120 km where the ion-neutral collision frequency ν_{in} is larger than the ion cyclotron frequency ω_{ci}, the dominant low-frequency mode is the helicon mode [*Greifinger*, 1972; *Papadopoulos et al.*, 1994; *Zhou et al.*, 1996]. This is the low-frequency ($\omega << \omega_{ci}$) branch of whistler wave and is carried by the electrons, since the ions are essentially immobile due to their strong coupling to the neutrals. In this region the Hall conductivity σ_H dominates over the Pedersen conductivity σ_P (Figure 1a). This altitude dependence of the conductivities has important consequences in the propagation of hydromagnetic waves and magnetosphere-ionosphere coupling [*Hughes*, 1983; *Lysak*, 1990; *Pilipenko*, 2012; *Waters et al.* 2013]. The shear Alfvén waves in the magnetosphere, e.g., the micropulsations, propagating into the ionosphere undergo changes in the ionosphere due the Hall conductance. In the high-latitude ionosphere, where the magnetic field is approximately vertical, the parallel current of the shear mode is closed by the Pedersen current and the inductive response of the ionosphere generates a compressional mode, which can propagate to the ground. The plasma conductance plays a similar role in the propagation of the wave generated by the heating in the ionosphere, but by changing the compressional to shear mode that propagate out to the magnetosphere, as discussed below.

The modulated heating produces a diamagnetic current in a localized heating region at altitudes ~300 km and excites magnetosonic waves which propagate isotropically. This can be viewed as waves generated by an oscillating field-aligned magnetic moment. In the Hall region these waves generate a local Hall current that excites shear Alfvén waves, which then propagate along the field lines to the ionospheric *E* region

and to the magnetosphere. This mechanism is referred to as ionospheric current drive (ICD) [*Papadopoulos et al.*, 2011a] and has been detected in HF heating experiments [*Papadopoulos et al.*, 2011b]. Numerical studies of Alfvén wave propagation in the ionosphere have been conducted by *Lysak* [1997], who developed a two-dimensional numerical model to study the propagation of waves in the 1 Hz band in the auroral zone (with vertical geomagnetic field). This model was later extended to three dimensions and to include the Earth's dipole magnetic field [*Lysak and Song*, 2001; *Lysak*, 2004].

The midlatitude ionosphere has similar plasma profiles as the auroral region, but the magnetic field geometry is significantly different in at least two ways (see Figure 1b): the field lines are oblique and curved. This leads to changes in the propagation characteristics of the low-frequency waves. Further, a wavefront propagating out of a heated region in the midlatitude ionosphere will intercept a wider area in the *E* region where the shear Alfvén waves are excited. The aim of this paper is to study the generation of ELF waves during HF heating of the midlatitude ionosphere and their propagation in the ionosphere and magnetosphere.

The paper is organized as follows. Section 2 describes the plasma model of the ionosphere for describing the plasma physical processes during HF heating and the numerical code, as well as the heating process and the excitation of ELF waves. The numerical results are discussed in section 3, where the differences of wave propagation at different frequencies are pointed out. Finally, the conclusions of the paper are presented in section 4.

2. Ionospheric Plasma Model and Simulation Setup

The ionospheric plasma has a quasi-equilibrium density profile, such as the Chapman profile, and the propagation of low-frequency waves ($\omega << \omega_{ci} << \omega_{ce}$) is described by using an MHD model of the plasma. In the ELF regime, the electron inertia can be neglected in the momentum equation,

$$0 = -\frac{e}{m_e}(\mathbf{E} - \mathbf{v}_e \times \mathbf{B}_0) - \nu_{\mathrm{en}}\mathbf{v}_e - \frac{\nabla P_e}{n_0}, \tag{1}$$

where $P_e(\mathbf{r}, t) = n_0 k_B T_e(\mathbf{r}, t)$ represents the modulated electron pressure due to local heating, $T_e(\mathbf{r}, t)$ is the electron temperature, k_B is the Boltzmann's constant, $\nu_{\mathrm{en}}(\mathbf{r})$ is the electron-neutral collision frequency, e is the magnitude of the electron charge, and m_e is the electron mass. For the modulated electron temperature, we use

$$T_e = T_{\mathrm{mod}} \tanh^2\left(\frac{t}{D_t}\right) \cos(\omega t) \exp\left[-\frac{r_\theta^2}{D_{r\theta}^2} - \frac{(h - h_{\mathrm{max}})^2}{D_h^2}\right], \tag{2}$$

where T_{mod} is the modulation amplitude of the electron temperature, D_t is the risetime, $D_{r\theta}$ and D_h are the widths of the heated region in the latitudinal and radial directions, $r_\theta = (R_E + h_{\mathrm{max}})(\theta - \theta_{\mathrm{max}})$ is the latitudinal distance to the heated region, $r_h = h - h_{\mathrm{max}}$ is the altitudinal distance to the heated region, $h = R - R_E$ is the altitude above ground, h_{max} is the altitude of the heated region, $\theta_{\mathrm{max}} = \arcsin\sqrt{(R_E + h_{\mathrm{max}})/(R_E L)}$ is the colatitudinal coordinate of the heated region, and ω is the modulation frequency. This setup centers the heated region on the L shell. In the simulations, we use $R_E = 6000$ km, $T_{\mathrm{mod}} = 2000$ K, $D_t = 0.5$ s, $D_{r\theta} = 40$ km, $D_h = 20$ km, and $h_{\mathrm{max}} = 300$ km, and $L = 1.6$. Similar to *Eliasson et al.* [2012], we have omitted the slow mean temperature increase, which will not contribute to the wave dynamics, and we have kept only the oscillating part of the electron temperature.

The ion fluid velocity $\mathbf{v}_i$ is governed by the ion momentum equation

$$\frac{\partial \mathbf{v}_i}{\partial t} = \frac{e}{m_i}(\mathbf{E} - \mathbf{v}_i \times \mathbf{B}_0) - \nu_{\mathrm{in}}\mathbf{v}_i\ , \tag{3}$$

where ν_{in} is the ion-neutral collision frequency and m_i is the ion mass. The electric and magnetic fields **E** and **B** are governed by Faraday and Ampère's laws

$$\nabla \times \mathbf{E} = -\frac{\partial \mathbf{B}}{\partial t} \tag{4}$$

and

$$\nabla \times \mathbf{B} = \mu_0 e n_0(\mathbf{r})(\mathbf{v}_i - \mathbf{v}_e). \tag{5}$$

Respectively, where μ_0 is the magnetic permeability in vacuum. The plasma is considered quasi-neutral with equal electron and ion number densities.

For the background magnetic field we use a dipole model $\mathbf{B}_0 = B_{0r}\,\hat{\mathbf{r}} + B_{0\theta}\,\hat{\boldsymbol{\theta}}$, where $\hat{\mathbf{r}}$ and $\hat{\boldsymbol{\theta}}$ are unit vectors in the radial and colatitudinal direction, respectively; in geomagnetic coordinates, $B_{0r} = -2\,B_{eq}R_E^3/R^3\cos\theta$ and $B_{0\theta} = -B_{eq}R_E^3/R^3\sin\theta$ are the respective magnetic field components, $B_{\rm eq} = 3.12\times10^{-5}$ T is the magnitude of the magnetic field at the magnetic equator; and $R = R_E + h$ is the total radius equal to the Earth's radius R_E plus altitude h.

For numerical convenience, the system of equations (1)–(5) are converted to a matrix form [*Eliasson et al*., 2012]

$$\frac{\partial \mathbf{A}}{\partial t} = -\mathbf{E} \tag{6}$$

and

$$\frac{\partial \mathbf{E}}{\partial t} = -\omega_{\rm ci}(\Gamma_{\rm in}+\Gamma_{\rm en})\mathbf{E} + \frac{\overline{\overline{\varepsilon}}^{-1}[\nabla\times(\nabla\times\mathbf{A})]}{\mu_0} - \frac{\overline{\overline{\mathbf{R}}}_e[\nabla\times(\nabla\times\mathbf{E})]}{\mu_0\,\tilde{\sigma}} + \left(\omega_{\rm ci}\overline{\overline{\mathbf{R}}}_i - \frac{\partial}{\partial t}\right)\frac{\nabla \mathrm{P_e}}{en_0}, \tag{7}$$

where we introduced the vector and scalar potentials $\mathbf{A}$ and ϕ via $\mathbf{B} = \nabla\times\mathbf{A}$ and $\mathbf{E} = -\nabla\phi - \partial\mathbf{A}/\partial t$, using the gauge $\phi = 0$. The $\overline{\overline{\mathbf{R}}}_e$ and $\overline{\overline{\mathbf{R}}}_i$ matrices (organizing the vectors as column vectors) are deduced from the electron and ion equations of motion (1) and (2) via the definitions $(\mathbf{v}_e\times\mathbf{B}_0 + m_e\,\nu_{en}\mathbf{v}_e/e)/B_0 \equiv \overline{\overline{\mathbf{R}}}_e\mathbf{v}_e$ and $(\mathbf{v}_i\times\mathbf{B}_0 - m_i\nu_{in}\,\mathbf{v}_i/e)/B_0 \equiv \overline{\overline{\mathbf{R}}}_i\mathbf{v}_i$, respectively. In doing so, the Cartesian coordinate system (x, y, z) of *Eliasson et al*. [2012] is here replaced by a spherical coordinate system (R, ϕ, θ) where R, ϕ, and θ are the radial, longitudinal, and colatitudinal coordinates, respectively. In the spherical coordinates, the magnitude of the dipole magnetic field is $B_0 = B_{\rm eq}(R_E/R)^3\sqrt{1+3\cos^2\theta}$. The $\overline{\overline{\mathbf{R}}}_e$ and $\overline{\overline{\mathbf{R}}}_i$ matrices are used to construct the inverse of an effective dielectric tensor $\overline{\overline{\varepsilon}}^{-1} = -\left(v_A^2/\varepsilon_0 c^2\right)\overline{\overline{\mathbf{R}}}_e\overline{\overline{\mathbf{R}}}_i$, where $v_A = c\omega_{\rm ci}/\omega_{\rm pi}$ is the Alfvén speed, and a conductivity tensor $\overline{\overline{\boldsymbol{\sigma}}} = \omega_{\rm ci}(\Gamma_{\rm in}+\Gamma_{\rm en})\overline{\overline{\boldsymbol{\varepsilon}}}$, where we have denoted $\Gamma_{\rm en} = \nu_{\rm en}/\omega_{\rm ce}$ and $\Gamma_{\rm in} = \nu_{\rm in}/\omega_{\rm ci}$. Here $\omega_{\rm ci} = e\,B_0/m_i$ and $\omega_{\rm ce} = e\,B_0/m_e$ are the ion and electron cyclotron frequencies, $\omega_{\rm pi} = (n_0\,e^2/\varepsilon_0\,m_i)^{1/2}$ and $\omega_{\rm pe} = (n_0e^2/\varepsilon_0\,m_e)^{1/2}$ are the ion and electron plasma frequencies, $\varepsilon_0 = c^2/\mu_0$ is the electric permittivity in vacuum, c is the speed of light in vacuum, and $\tilde{\sigma} = \varepsilon_0\omega_{\rm pe}^2/\omega_{\rm ce}$. The simulations are conducted in a domain in the north-south plane in the spherical coordinates with the simulation domain covering $R = R_E + 100$ km to $R_E + 4000$ km in the radial direction and a 90° wide angular region in the colatitudinal direction centered at the foot of the $L = 1.6$ shell, i.e., $\arcsin\left(1/\sqrt{L}\right) - 45° \le \theta \le \arcsin\left(1/\sqrt{L}\right) + 45°$. The simulation domain was resolved with 500 cells in the radial direction and 460 cells in the colatitudinal direction. A centered second-order difference scheme was used in the radial direction and a pseudo-spectral method with periodic boundary conditions in the colatitudinal direction. The simulations were stopped before the waves reached the simulation boundaries in the colatitudinal direction, hence eliminating the effects of the artificial periodic boundary conditions. First-order outflow boundary conditions were used at the top boundary in the radial direction [see *Eliasson et al*., 2012]. At the lower boundary between the plasma and free space at $R = R_E + 100$ km, the boundary conditions were obtained by assuming continuity of the horizontal components of the electric field and vector potential, and their radial derivatives. In free space, we have assumed infinite speed of light and that there are no electric charges or currents, while the ground at $R = R_E$ is perfectly conducting, so that analytic approximations for the free space electromagnetic fields can be used [see *Eliasson et al*., 2012].

The conductivity $\sigma_\parallel$ along the magnetic field is determined by the electron and ion mobilities, and when it has high values the parallel electric field is shorted. The Hall conductivity σ_H dominates over the Pedersen conductivity σ_P in the D and E regions, and the reverse is the case at higher altitudes. For one ion species, the parallel, Pedersen, and Hall conductivity, respectively, are given by $\sigma_\parallel = \tilde{\sigma}\left(\Gamma_{\rm en}^{-1} + \Gamma_{\rm in}^{-1}\right)$, $\sigma_P = \tilde{\sigma}\left[\,\Gamma_{\rm en}/\left(1+\Gamma_{\rm en}^2\right) + \Gamma_{\rm in}/\left(1+\Gamma_{\rm in}^2\right)\right]$, and $\sigma_H = \sigma\left[\,1/\left(1+\Gamma_{\rm en}^2\right) - 1/\left(1+\Gamma_{\rm in}^2\right)\,\right]$, where $\tilde{\sigma} = \varepsilon_0\omega_{\rm pe}^2/\omega_{\rm ce}$, and we have denoted $\Gamma_{\rm en} = \nu_{\rm en}/\omega_{\rm ce}$ and $\Gamma_{\rm in} = \nu_{\rm in}/\omega_{\rm ci}$.

$$\sigma_P = e^2\left[\frac{n_e\nu_{\rm en}}{m_e\left(\nu_{\rm en}^2+\omega_{\rm ce}^2\right)} + \sum_i \frac{n_i\nu_{\rm in}}{m\left(\nu_{\rm in}^2+\omega_{\rm ci}^2\right)}\right] \tag{8}$$

$$\sigma_H = e^2\left[\frac{n_e\omega_{\rm ce}}{m_e\left(\nu_{\rm en}^2+\omega_{\rm ce}^2\right)} - \sum \frac{n_i\omega_{\rm ci}}{m_i\left(\nu_{\rm in}^2+\omega_{\rm ci}^2\right)}\right], \tag{9}$$

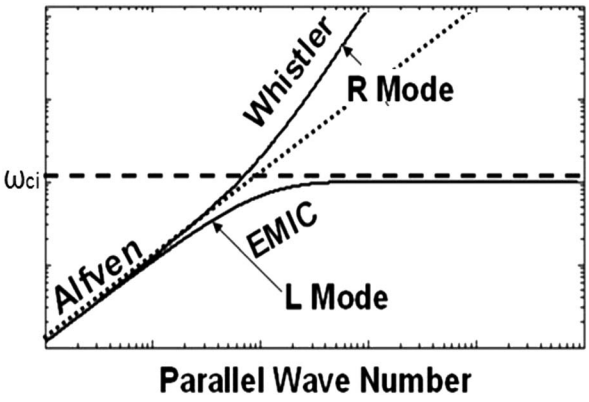

Figure 2. Sketch of wave modes propagating parallel to the magnetic field.

$$\sigma_{P,e} = e^2 \frac{n_e \nu_{en}}{m_e\left(\nu_{en}^2 + \omega_{ce}^2\right)}, \tag{10}$$

$$\sigma_{H,e} = e^2 \frac{n_e \omega_{ce}}{m_e\left(\nu_{en}^2 + \omega_{ce}^2\right)}, \tag{11}$$

$$\sigma_{||} = e^2\left(\sum_i \frac{n_i}{m_i \nu_{in}} + \frac{n_e}{m_e \nu_{en}}\right), \tag{12}$$

where $\sigma_{||,e} = e^2 n_e/(m_e \nu_{en})$. The plasma dielectric function ε is given by

$$\varepsilon = \frac{c^2}{V_A^2(z)\left[1 + \nu_{in}^2(z)/\omega_{ci}^2\right]}, \tag{13}$$

where $V_A = B/\sqrt{\mu_o n_i m_i}$ is the Alfvén speed.

The dispersion relation for collisionless obliquely propagating ELF Alfvén waves is

$$\left(\omega^2 - v_A^2 k^2\right)\left(\omega^2 - v_A^2 k_{||}^2\right) - \frac{\omega^2}{\omega_{ci}^2} v_A^4 k^2 k_{||}^2 = 0, \tag{14}$$

where $k^2 = k_{||}^2 + k_{\perp}^2$. The more general case including collisions is discussed by *Eliasson et al.* [2012]. For perpendicular propagation ($k_{||} = 0$) the solution of equation (14) yields the compressional or magnetosonic waves with dispersion relation

$$\omega^2 - v_A^2 k_{\perp}^2 = 0. \tag{15}$$

On the other hand, for parallel propagation ($k = k_{||}$) the dispersion relation becomes

$$\omega^2 \mp v_A^2 k_{||}^2 \frac{\omega}{\omega_{ci}} - v_A^2 k_{||}^2 = 0 \tag{16}$$

For large wave numbers $k \gtrsim c/\omega_{pi}$ the shear Alfvén mode splits into two modes (see Figure 2), viz., the right-hand circularly polarized (R-mode) whistler and the left-hand circularly polarized (L-Mode) electromagnetic ion cyclotron (EMIC) mode, which is also known as the Alfvén-cyclotron mode. While the whistler mode can propagate at frequencies $\omega > \omega_{ci}$ at large wave numbers, the EMIC propagates always at frequencies $\omega < \omega_{ci}$ and has a resonance at ω_{ci} for large wave numbers.

The HF heating of the ionosphere with ground transmitters leads to many physical processes with a wide range of space and time scales. On the scales relevant to the low-frequency waves, the processes due to HF heating result in a local hot spot whose size and duration are determined mainly by the beam size and modulation frequency. For the proposed studies the processes at the short scales are not directly relevant and a volume averaged picture is used in this model. Thus, the heated region will be modeled as a region of enhanced electron pressure $P_e = nT_e$ (T_e in energy units) and is assumed to have a pancake shape with Gaussian profiles in the radial and latitudinal directions. In this case the heating term in the Ohm's law is $-\nabla P_e$ in equations (1) and (7). This pressure gradient in the magnetized plasma leads to the usual diamagnetic current given by

$$\mathbf{J} = \mathbf{B} \times \nabla P_e / B^2, \tag{17}$$

which has a time variation due to the modulated nature of the heating. For a scalar pressure the only the perpendicular component, viz., $\nabla_{\perp} T_e$, contributes to the diamagnetic current due to the modulated heating. This model represents the average effect of the wide range of processes at short scales and is, in general, adequate for the study of wave generation and propagation by modulated HF heating. Phenomena such as descending plasma layer [*Pedersen et al.*, 2010; *Mishin and Pedersen*, 2011], whose characteristics depend on the parameters of the HF heater and local ionospheric conditions, can have space and time scales that would require more detailed representation of the heated region.

3. ELF Wave Generation and Propagation in the Ionosphere

The wave propagation model described above yields a framework for the simulation of low-frequency waves in the ionosphere. The heated region is centered at $L = 1.6$, and the modulation of the HF waves at

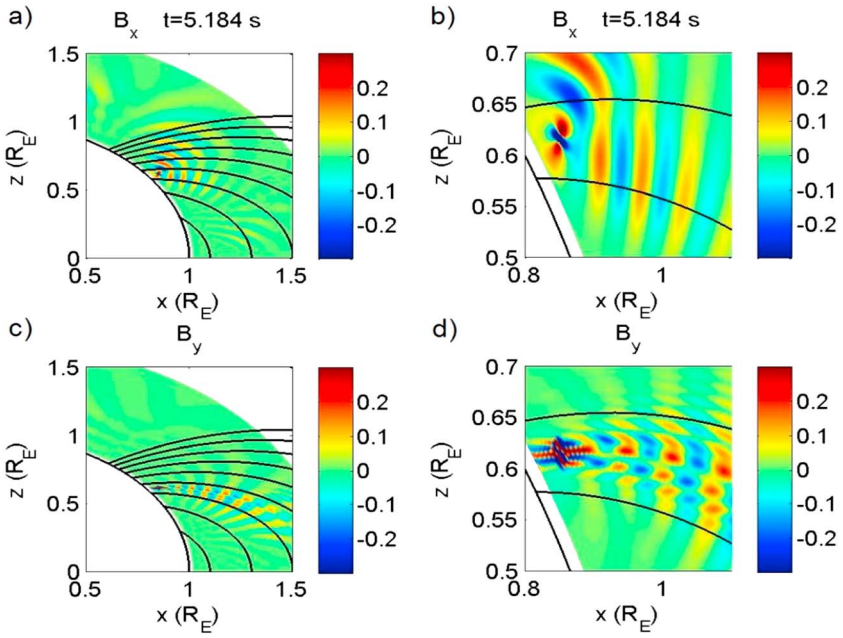

Figure 3. Wave magnetic field (pT) of ELF waves excited in ionospheric heating by HF waves modulated at 2 Hz. (a and b) The B_x component is associated with magnetosonic waves, while (c and d) the B_y component is associated with shear Alfvén waves. Figures 3b and 3d show a close-up of Figures 3a and 3c, respectively, in the heated region.

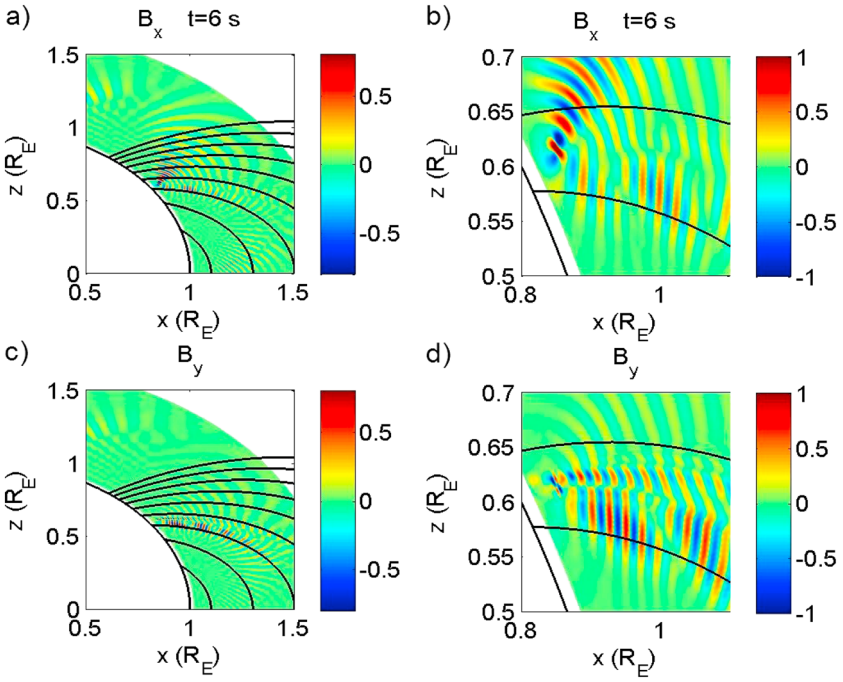

Figure 4. Wave magnetic field (pT) of 5 Hz ELF waves excited by modulated ionospheric heating. As in Figure 3, (a and b) the B_x component is associated with magnetosonic waves, while (c and d) the B_y component is associated with shear Alfvén waves. Figures 4b and 4d are close-ups of the respective the heating regions.

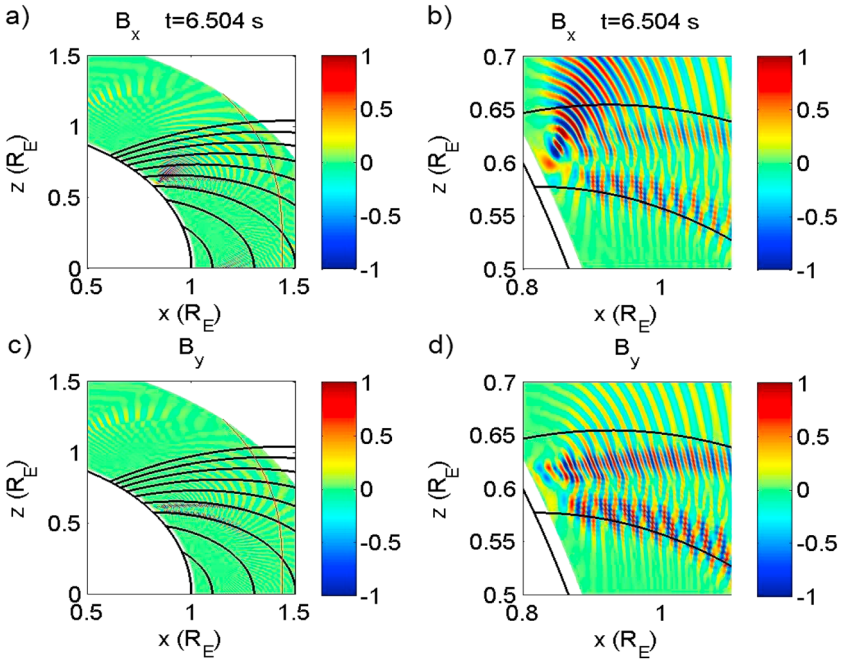

Figure 5. Wave magnetic field (pT) of 10 Hz ELF waves excited by modulated ionospheric heating. (a and b) The B_x component is associated with magnetosonic waves, while (c and d) the B_y component is associated with shear Alfvén waves. Figures 5b and 5d show a close-up of Figures 5a and 5c, respectively, in the heated region. The location of the ion cyclotron resonance at 10 Hz is indicated with a thin line in Figures 5a and 5c.

frequencies $f = 2$ Hz, 5 Hz, and 10 Hz is studied. The simulation runs up to 12 s using 4×10^5 time steps. The ionosphere is represented by a Chapman profile, with a peak density of 5×10^{10} m^{-3} at about 500 km, corresponding to a minimum of the Alfvén speed of $v_A \approx 900$ km/s. An overview of ELF wave generation and propagation at frequencies 2 Hz, 5 Hz, and 10 Hz are shown in Figures 3–5, respectively.

As seen in Figures 3 and 4, both magnetosonic and shear Alfvén waves are generated by the modulated ionospheric heating. At frequencies much below the ion cyclotron frequency (on the order 10–50 Hz depending on altitude and latitude), the shear Alfvén wave propagates primarily along the magnetic field lines. Magnetosonic waves (visible as B_x) are created by ICD and propagate at large angles to the geomagnetic field lines upward to the magnetosphere (see Figures 3a and 3b and 4a and 4b) and downwards to E region. Somewhat below the $L = 1.6$ magnetic field line extending from the heated region are whistler mode waves (cf. Figure 4d). These waves are not created at the heated location but at the Hall region at the bottom of the ionosphere where magnetosonic waves have been mode converted to helicon waves propagating to higher altitudes as whistler waves. Near the heated region there is also a direct generation of EMIC waves.

As the wave frequency becomes comparable to the ion cyclotron frequency, the splitting of the shear Alfvén wave into the whistler and EMIC branches become more pronounced (cf. Figure 2). The whistler wave is characterized by a longer wavelength and higher propagation speed than the EMIC wave at a given frequency. The shorter wavelength EMIC waves and longer wavelength whistler waves are clearly distinguished in Figure 5d, while the magnetosonic wave propagating at larger angles to the geomagnetic field is visible in Figure 5b.

The propagation of the EMIC toward the ion cyclotron resonance at high altitudes is of particular interest since they play an important role in plasma heating in the magnetosphere, The resonance surface is indicated by thin lines in Figures 5a and 5c. Figure 6 shows contours of the EMIC waves for selected values of the wavelength for parallel propagation at 10 Hz.

The 10 Hz EMIC waves cannot propagate beyond ion cyclotron resonance layer where their wavelength goes to zero, and the EMIC wave energy will pile up near the resonance. The amplitude of the wave magnetic field can be estimated from the conservation of energy. For simplicity we consider propagation parallel to the

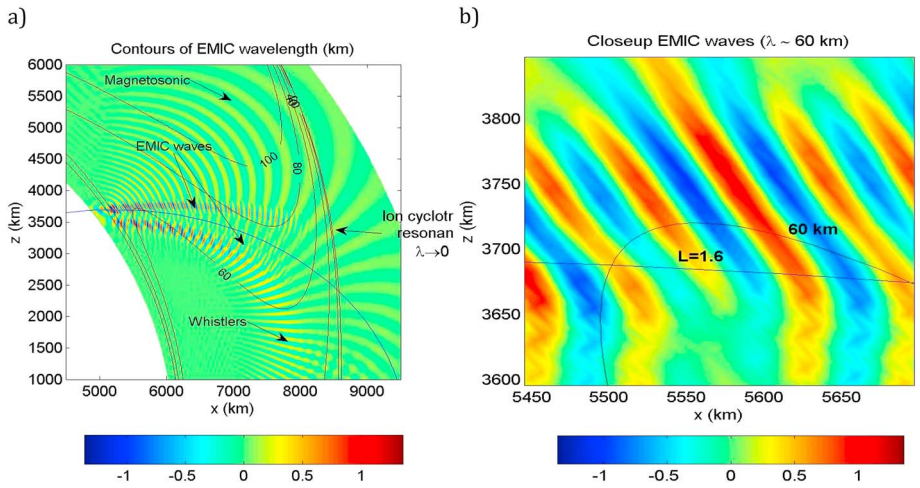

Figure 6. (a) Propagation of 10 Hz EMIC waves toward the ion cyclotron resonance, showing the B_y component of the wave magnetic field (pT). Contours indicate the wavelength of the EMIC wavelength, which goes to zero as the EMIC wave approaches the altitude of the resonance. (b) Close-up of EMIC waves with a wavelength of about 60 km.

magnetic field, $\mathbf{k} = \mathbf{k}_{\|}$. The wave energy density W consists of a sum of magnetic wave energy density $B^2/(2\mu_0)$ and of ion kinetic energy density $n_0\, m_i v_i^2/2$. From Ampère's law we have $\mathbf{k}_{\|} \times \mathbf{B} = \mu_0 e n_0 \mathbf{v}_i$ when $ck_{\|}/\omega_{pe} \gg 1$. Therefore, instead of the energy density $W = B^2/(2\mu_0)$, we will instead have $W = n_0\, m_i\, v_i^2/2 = \left(c^2 k_{\|}^2/\omega_{pi}^2\right) B^2/(2\mu_0)$. Energy conservation requires that the wave intensity $I = v_{gr} W \approx$ constant, where $v_{gr} = \partial\omega/\partial k_{\|}$ is the group speed. For $ck_{\|}/\omega_{pe} \gg 1$ we have the EMIC wave frequency $\omega \approx \omega_{ci}\left(1 - \omega_{pi}^2/\left(c^2 k_{\|}^2\right)\right)$ and group velocity $v_g = 2\omega_{ci}\omega_{pi}^2/\left(c^2 k_{\|}^3\right)$, hence $I = v_{gr} W = (2\omega_{ci}/k_{\|}) B^2/(2\mu_0)$. Solving for B, we find

$$B \sim \text{constant} \times \sqrt{\frac{\omega_{pi}}{\omega_{ci}}} \left(1 - \frac{\omega}{\omega_{ci}}\right)^{-1/4},$$

which predicts an increase of the wave magnetic field amplitude near the resonance. These waves suffer cyclotron damping, which may become important at very small wavelengths when the phase velocity $\approx \omega_{ci}/k_{\|} \approx v_A \sqrt{1 - \omega/\omega_{ci}}$ becomes comparable to the ion thermal speed.

4. Summary

The excitation and propagation of ELF waves in the midlatitude ionosphere and magnetosphere during HF heating are simulated using a MHD model. The simulation model uses a realistic profile of ionospheric plasma, along with the Earth's magnetic dipole field. The latter is an important element in the modeling of the midlatude ionosphere because of the geometrical effects in wave propagation. The simulation results show direct generation of EMIC waves at the source region as well as mode conversion of magnetosonic waves through the excitation of Hall currents in the *E* region. The waves are generated at the modulation frequency of the HF radio waves by the ionospheric current drive, which does not involve a quasi-steady current in the ionosphere, viz., an electrojet current [*Papadopoulos et al.*, 2011a, *Sharma et al.*, 2016]. This mechanism of wave generation was found to be effective in the *F* region ionosphere in the high latitudes, with the auroral electrojet in the *D*/*E* region. In the midlatitudes with no quasi-steady current system, this mechanism is expected to be a dominant process for exciting ELF waves. The results are thus directly relevant for the heating experiments with the Arecibo facility, which have been commissioned recently.

The simulation results are relevant to in situ satellite measurements near the heating site and can be used to study energetic particle precipitation from radiation belts through resonant pitch angle scattering. In the higher frequency range the excited waves are the EMIC waves, which play an important role in the plasma heating in the magnetosphere. A study of the interaction of hydromagnetic waves with trapped protons in the inner magnetosphere shows that the proton precipitation can be enhanced significantly [*Shao et al.*, 2009]. The ELF waves

excited by ionospheric heating, in particular the EMIC waves, are a possible source of the waves that can lead to such effects. However, the simulations show that the waves do not propagate beyond the resonance layer, and thus may limit the interaction with the energetic particles in the magnetosphere. It should be noted that the simulations consider an ionospheric plasma with singly charged oxygen as the ion specie. At higher altitudes, viz., above 1000 km, protons become the dominant ion specie and a more complete model should include a mix of oxygen ions and protons, with altitude dependent densities. With such a model the oxygen ions will have a dominant role in the wave generation in the *F* layer, as in the present model, and as the hydromagnetic waves propagate to higher altitudes its propagation characteristics will be governed mainly by the protons. The resonance layers in a plasma with protons as the main ion specie will be farther away in the radiation belt, and thus, the extent of the interaction of the EMIC waves with protons should be assessed with a more detailed study.

The simulations presented here were carried out in a domain defined in the spherical coordinates, which is suitable for the dipole magnetic field geometry. However, the realistic geometry is more complicated due to the dipole tilt and the manner in which the variation of the vertical magnetic field with height deviates from the radial stratification of the ionosphere. The wave propagation in the midlatitudes formulated using nonorthogonal flux coordinates [*Lysak*, 2004] treats these effets properly and provides a more detailed framework. However, the main results of the ELF wave excitation presented here is not expected to be significantly different when analyzed in the more complicated nonorthogonal system.

The key element in the excitation and propagation of ELF waves is the altitude dependence of the plasma conductivity, viz., the Hall and Pedersen conductances. The role of this feature in magnetosphere-ionosphere coupling has been actively studied [e.g., see *Hughes*, 1983; *Lysak*, 1990, 2004; *Pilipenko*, 2012; *Waters et al*. 2013]. The shear Alfvén waves in the magnetosphere, e.g., the micropulsations, propagating into the ionosphere undergo changes in the ionosphere due the varying conductance. In the high-latitude ionosphere, the parallel current of the shear mode is closed by the Pedersen current and the inductive response of the ionosphere generates a compressional mode, which can propagate to the ground. On the other hand, the excitation of ELF waves in ionospheric heating presented in this paper follows the opposite sequence: first exciting the compressional mode and then the shear mode.

The HAARP facility has enabled new advances in ionospheric physics, e.g., excitation of ELF waves [*Papadopoulos et al*., 2011a, 2011b; *Moore et al*., 2013], formation of ducts and ion up flows [*Kosch et al*., 2010, *Milikh et al*., 2010], and descending artificial ionospheric layers [*Pedersen et al*., 2010]. The new plasma layers are results of enhanced ionization by electrons, which are accelerated to suprathermal speeds by turbulence resulting from HF heating [*Mishin and Pedersen*, 2011]. Simulations of wave processes in the presence of ducts using a Vlasov code show stochastic electron heating due to upper hybrid and Bernstein wave turbulence (A. Najmi et al., Theoretical studies of fast stochastic electron heating near the upper hybrid layer, submitted to *Radio Science*, 2016) and thus provide insights into the kinetic processes in HF heating. Experiments with the Arecibo heating facility are expected to yield more details of these phenomena in the midlatitude ionosphere, and those planned considering detection of the signatures of heating-induced processes by spacecraft such as the Van Allen Probes can provide deeper insight into the effects on energetic particles in the radiation belt.

Acknowledgments
The research at the University of Maryland is supported by NSF grant AGS-1158206 and AFOSR/MURI grant FA95501410019. B.E. acknowledges the UK Engineering and Physical Sciences Research Council for supporting this work under grant EP/M009386/1. The paper contains no observational data, and for the simulation data please contact ssh@astro.umd.edu.

References

Bernhardt, P. A., C. A. Tepley, and L. M. Duncan (1989), Airglow enhancements associated with plasma cavities formed during ionospheric heating experiments, *J. Geophys. Res.*, *94*, 907.

Eliasson, B., C.-L. Chang, and K. Papadopoulos (2012), Generation of ELF and ULF electromagnetic waves by modulated heating of the ionospheric F2 region, *J. Geophys. Res.*, *117*, A10320, doi:10.1029/2012JA017935.

Greifinger, C. (1972), Ionospheric propagation of oblique hydromagnetic plane waves at micropulsation frequencies, *J. Geophys. Res.*, *77*, 2377–2391, doi:10.1029/JA077i013p02377.

Gurevich, A., A. Lukyanov, and K. Zybin (1996), Anomalous absorption of powerful radio waves on the striations developed during ionospheric modification, *Phys. Lett. A*, *211*, 363–372.

Guzdar, P. N., N. A. Gondarenko, K. Papadopoulos, G. M. Milikh, A. S. Sharma, P. Rodriguez, Y. V. Tokarev, Y. I. Belov, and S. L. Ossakow (2000), Diffraction model of ionospheric irregularity-induced heater-wave pattern detected on the WIND satellite, *Geophys. Res. Let.*, *27*, 317–320.

Hughes, W. J. (1983), Hydromagnetic waves in the magnetosphere, *Rev. Geophys. Space Phys.*, *21*, 508–520.

Kosch, M., Y. Ogawa, M. Rietveld, S. Nozawa, and R. Fujii (2010), An analysis of pump-induced artificial ionospheric ion upwelling at EISCAT, *J. Geophys. Res.*, *115*, A12317, doi:10.1029/2010JA015854.

Leyser, T. B. (2001), Stimulated electromagnetic emissions by high-frequency electromagnetic pumping of the ionospheric plasma, *Space Sci. Rev.*, *98*, 223–328.

Lysak, R. L. (1990), Electrodynamic coupling of the magnetosphere and ionosphere, *Space Sci. Rev.*, *52*(1–2), 33–87.
Lysak, R. L. (1997), Propagation of Alfvén waves through the ionosphere, *Phys. Chem. Earth*, *22*, 757–766.
Lysak, R. L., and Y. Song (2001), A three-dimensional model of the propagation of Alfvén waves through the auroral ionosphere: First results, *Adv. Space Res.*, *28*(5), 813–822.
Lysak, R. L. (2004), Magnetosphere-ionosphere coupling by Alfvén waves at midlatitudes, *J. Geophys. Res.*, *109*, A07201, doi:10.1029/2004JA010454.
Milikh, G., E. Mishin, I. Galkin, A. Vartanyan, C. Roth, and B. Reinisch (2010), Ion outflows and artificial ducts in the topside ionosphere at HAARP, *Geophys. Res. Lett.*, *37*, L18102, doi:10.1029/2010GL044636.
Mishin, E., W. Burke, and T. Pedersen (2005), HF-induced airglow at magnetic zenith: Theoretical considerations, *Ann. Geophys.*, *23*, 47–53.
Mishin, E., and T. Pedersen (2011), Ionizing wave via high-power HF acceleration, *Geophys. Res. Lett.*, *38*, L01105, doi:10.1029/2010GL046045.
Moore, R. C., S. Fujimaru, D. A. Kotovsky, and M. Golkowski (2013), Observations of ionospheric ELF and VLF wave generation by excitation of the thermal cubic nonlinearity, *Phys. Rev. Lett.*, *111*, 235007.
Papadopoulos, K., A. S. Sharma, and C. L. Chang (1989), On the efficient operation of a plasma ELF antenna driven by modulation of ionospheric currents, *Comm. Plasma Phys. and Cont. Fus.*, *13*, 1–17.
Papadopoulos, K., H.-B. Zhou, and A. S. Sharma (1994), The role of helicon waves magnetospheric and ionospheric physics, *Comm. Plasma Phys. and Cont. Fus.*, *15*, 321.
Papadopoulos, K., N. Gumerov, X. Shao, C. L. Chang, and I. Doxas (2011a), HF driven currents in the ionosphere, *Geophys. Res. Lett.*, *38*, L12103, doi:10.1029/2011GL047368.
Papadopoulos, K., C.-L. Chang, J. Labenski, and T. Wallace (2011b), First demonstration of HF-driven ionospheric currents, *Geophys. Res. Lett.*, *38*, L20107, doi:10.1029/2011GL049263.
Pedersen, T. R., and E. A. Gerken (2005), Creation of visible artificial optical emissions in the aurora by high-power radio waves, *Nature*, *433*, 498, doi:10.1038/nature03243.
Pedersen, T., B. Gustavsson, E. Mishin, E. Kendall, T. Mills, H. C. Carlson, and A. L. Snyder (2010), Creation of artificial ionospheric layers using high-power HF waves, *Geophys. Res. Lett.*, *37*, L02106, doi:10.1029/2009GL041895.
Pilipenko, V. A. (2012), Impulsive coupling between the atmosphere and ionosphere/magnetosphere, *Space Sci. Rev.*, *168*, 533–550, doi:10.1007/s11214-011-9859-8.
Shao, X., K. Papadopoulos, and A. S. Sharma (2009), Control of the energetic proton flux in the inner radiation belt by artificial means, *J. Geophys. Res.*, *114*, A07214, doi:10.1029/2009JA014066.
Sharma, A. S., B. Eliasson, G. M. Milikh, A. Najmi, K. Papadopoulos, X. Shao, and A. Vartanyan (2016), Low-frequency waves in HF heating of the ionosphere, in *Low-Frequency Waves in Space Plasmas*, *Geophysical Monograph 216*, 1st ed., edited by A. Keiling, D.-H. Lee, and V. Nakariakov, pp. 31–49, AGU, Washington, D. C.
Stubbe, P., H. Kopka, and R. L. Dowden (1981), Generation of ELF and VLF waves by Polar Electrojet modulation: Experimental results, *J. Geophys. Res.*, *86*, 9073–9078, doi:10.1029/JA086iA11p09073.
Stubbe, P. (1996), Review of ionospheric modification experiments at Tromso, *J. Atmos. Sol. Terr. Phys.*, *58*, 349–368, doi:10.1016/0021-9169(95)00041-0.
Waters, C. L., R. L. Lysak, and M. D. Sciffer (2013), On the coupling of fast and shear Alfvén wave modes by the ionospheric Hall conductance, *Earth Planets Space*, *65*, 385–396, doi:10.5047/eps.2012.08.002.
Zhou, H. B., K. Papadopoulos, A. S. Sharma, and C.-L. Chang (1996), Electron-magnetohydrodynamic response of a plasma to an external current pulse, *Phys. Plasmas*, *3*, 1484, doi:10.1063/1.872009.